Nanomed Res J 10(4):416-429, Autumn 2025

RESEARCH ARTICLE

Chitosan Nanoparticle Hydrogels with *Mentha piperita* Essential Oil and Menthol: Preparation, Antibacterial Efficacy, and Molecular Docking Analysis

Pardis Parhizkar[1,2], Mohsen Safaei[3], Zahra Montaseri[4], Roghayeh Heiran[5], Malihe GhalkarYazd[3], Maedeh Nasira[6], Mahbod Fazlali[6], Mahmoud Osanloo[7*]

[1] Student Research Committee, Fasa University of Medical Sciences, Fasa, Iran

[2] Department of Medicine, School of Medicine, Fasa University of Medical Sciences, Fasa, Iran.

[3] Department of Medical Biotechnology, School of Advanced Technologies in Medicine, Fasa University of Medical Sciences, Fasa, Iran.

[4] Department of Infectious Diseases, School of Medicine, Fasa University of Medical Sciences, Fasa, Iran.

[5] Estahban Higher Education Center- Shiraz University, Estahban, Iran

[6] Noncommunicable Disease Research Center, Fasa University of Medical Sciences, Fasa, Iran

[7] Department of Medical Nanotechnology, School of Advanced Technologies in Medicine, Fasa University of Medical Sciences, Fasa, Iran

ARTICLE INFO

Article History:
Received 08 Sep 2025
Accepted 18 Nov 2025
Published 01 Dec 2025

Keywords:
Major component
Herbal Medicine
Essential oil

ABSTRACT

Antibiotic-resistant skin infections caused by pathogens necessitate the development of novel therapeutic strategies to combat these infections. Natural agents such as *Mentha piperita* essential oil (EO) and its primary component, menthol, present promising alternatives. In this study, chitosan nanoparticles loaded with EO or menthol were synthesized via ultrasound-assisted ionic gelation and incorporated into hydrogels using HPMC as the gelling agent. Formulations were characterized by DLS, ATR-FTIR, and rheometry. Antibacterial efficacy was evaluated against *Escherichia coli* and *Staphylococcus aureus* using the AATCC 100 method. Molecular docking predicted menthol's binding affinity to key bacterial proteins. GC-MS confirmed menthol (31%) as the major EO component. Nanoparticles were 179-195 nm with a positive zeta potential. ATR-FTIR verified encapsulation, and rheology confirmed shear-thinning behavior. Nanoparticle-based hydrogels demonstrated significantly enhanced antibacterial activity, achieving near-total bacterial suppression. Docking results indicated strong binding of menthol to key bacterial targets, supporting its antimicrobial mechanism. Chitosan nanoparticle-based hydrogels encapsulating *M. piperita* EO and menthol are a highly effective, rheologically favorable platform for combating resistant bacterial skin infections.

How to cite this article
ParhizkarP., Safaei M., Montaseri Z., Heiran R., GhalkarYazd M., Nasira M., Fazlali M., Osanloo M. Chitosan Nanoparticle Hydrogels with Mentha piperita Essential Oil and Menthol: Preparation, Antibacterial Efficacy, and Molecular Docking Analysis. Nanomed Res J, 2025; 10(4): 416-429. DOI: 10.22034/nmrj.2025.04.009

INTRODUCTION

Bacterial skin infections, particularly those caused by *Escherichia coli* and *Staphylococcus aureus*, represent a significant global health challenge, especially in healthcare settings. These pathogens are a leading cause of healthcare-associated infections (HAIs), imposing a considerable socioeconomic burden due to prolonged treatment durations and escalating healthcare costs [1, 2].

Conventional antibiotic treatments against these bacteria face considerable challenges. Sophisticated bacterial resistance mechanisms, such as efflux pump systems that actively expel antimicrobial compounds, combined with the protective nature of biofilms, can increase bacterial

* Corresponding Author Email: *m.osanloo@fums.ac.ir*

tolerance by 10- to 1,000-fold [3, 4]. This has spurred the exploration of alternative antimicrobial strategies. *Mentha piperita* essential oil (EO) and its principal component, menthol, have demonstrated broad-spectrum antimicrobial activity against both Gram-positive and Gram-negative bacteria, as well as anti-inflammatory properties, making them promising candidates for managing skin infections [5-7]. Menthol, a naturally occurring chemical found in numerous plant species, has garnered considerable interest due to its unique pharmacological properties. Menthol, widely recognized for its aromatic and cooling properties, demonstrates a diverse range of biological actions that highlight its medicinal potential [8-10]. To rationally guide their application, computational approaches such as molecular docking can provide valuable insights into the potential mechanisms of action by predicting the binding interactions and affinity of menthol with key bacterial proteins [11, 12].

Furthermore, EOs and their constituents are inherently lipophilic and volatile, which limits their direct topical application and efficacy. To enhance their usability, these compounds require formulation into hydrophilic delivery systems. Hydrogels, three-dimensional polymeric networks that can absorb large amounts of water while maintaining structural integrity, are among the most suitable platforms for topical applications due to their high biocompatibility, ease of application, and capacity for controlled release [13, 14].

A promising approach in hydrogel formulation involves polymer combination. In this strategy, the EO or active component is first dispersed within a bioactive polymer, such as chitosan. A secondary polymer is then used to gel the system, leveraging the synergistic properties of both materials [15, 16]. Chitosan, a natural polysaccharide derived from chitin, is widely recognized for its biocompatibility, biodegradability, and intrinsic antimicrobial properties [17]. Hydroxypropyl methylcellulose (HPMC), a semi-synthetic polymer, is another excellent candidate, known for its superior gel-forming capacity, biocompatibility, and stability in pharmaceutical formulations [18, 19]. Furthermore, with advancements in nanotechnology, loading bioactive compounds into nanostructures prior to hydrogel incorporation has emerged as a powerful strategy to enhance stability, bioavailability, and provide sustained release, leading to the development of efficient nanoparticle-based hydrogels [20, 21].

In this study, we developed and characterized advanced hydrogels containing *M. piperita* EO and menthol. Chitosan/HPMC hydrogels and nanoparticle-based chitosan/HPMC hydrogels containing either the EO or menthol (Chi/HPMC-EO, Chi/HPMC-Menthol, ChiNP/HPMC-EO, and ChiNP/HPMC-Menthol) were prepared, and their antibacterial efficacy was evaluated against *E. coli* and *S. aureus*. Following the promising results from these antibacterial assays, we performed molecular docking simulations to gain deeper insight into the molecular basis of the observed activity. Specifically, the interactions of menthol with a selection of vital protein targets from *S. aureus* and *E. coli* were investigated..

MATERIALS AND METHODS

Materials

Chitosan (medium molecular weight, 75–85% deacetylation), menthol, tween 20, and hydroxypropyl methylcellulose (HPMC) were obtained from Merck Chemicals (Germany). Bark-extracted *M. piperita* EO was supplied by Tabib Daru Company (Iran). Bacterial strains, namely *S. aureus* (ATCC 25923) and *E. coli* (ATCC 25922), were provided by the Paesture Institute (Iran).

M. piperita EO Analysis Using GC-MS

The chemical composition of *M. piperita* EO was characterized using gas chromatography-mass spectrometry (GC-MS). Analysis was performed on an Agilent 6890 gas chromatograph coupled with an Agilent 5973N mass selective detector. Volatile constituents were separated on an HP-5ms capillary column with helium as the carrier gas. The oven temperature was initially set at 50°C (held for 3 minutes) and then increased linearly at a rate of 10°C/min until it reached 300°C. Mass spectra were recorded in electron impact ionization mode over a mass range of 35–450 m/z, and compound identification was achieved by matching the obtained spectra with reference libraries (Wiley and Adams).

Preparation and Characterization of Chitosan nanoparticle and Chitosan solution-based HPMC hydrogels

Because menthol is difficult to disperse uniformly in aqueous media, ultrasound was also used in the ionic gelation method [22]. For both active compounds, 0.25% w/v of either *M.*

piperita EO or menthol was emulsified with 0.5% w/v of Tween 20 by stirring continuously at room temperature for 5 min (2000 rpm). Next, 4.5 mL of a 0.25% (w/v) chitosan solution—prepared by dissolving chitosan in 1% (v/v) acetic acid—was added dropwise and then was sonicated for 30 min using a bath sonicator (37 kHz) to ensure uniform dispersion of *M. piperita* EO or menthol into the polymeric matrix. For nanoparticle formation, sodium tripolyphosphate (TPP) solution (0.04% w/v) was added to reach 5 mL to initiate ionic crosslinking, and the mixture was stirred (2000 rpm) for an additional 40 minutes to complete nanoparticle formation. Subsequently, HPMC powder (1.5% w/v) was gradually incorporated into the prepared chitosan nanoparticles with continuous stirring (2000 rpm) overnight at room temperature to achieve a homogeneous mixture with optimal viscoelastic properties. The prepared samples were named ChiNP/HPMC-EO and ChiNP/HPMC-Menthol.

The hydrogel based on chitosan solutions was prepared similarly, with the same amount of distilled water used instead of the TPP solution; these were named Chi/HPMC-EO and Chi/HPMC-Menthol. Additionally, to investigate the antibacterial properties of the components in the prepared hydrogels, blank hydrogels, i.e., those without *M. piperita* EO or menthol, were prepared using the same method; they were named ChiNP/HPMC and Chi/HPMC.

The resultant chitosan nanoparticles were analyzed using Dynamic Light Scattering (DLS) to confirm nanoparticle sizes below 200 nm and a narrow particle size distribution (SPAN < 1). In addition, Attenuated Total Reflectance-Fourier-Transform InfraRed (ATR-FTIR) spectroscopy was performed on multiple samples—namely A: *M. piperita* EO, B: menthol, C: HPMC, D: Chi/HPMC, E: Chi/HPMC-EO, F: Chi/HPMC-Menthol, G: ChiNP/HPMC, H: ChiNP/HPMC-EO, and I: ChiNP/HPMC-Menthol—to verify successful encapsulation and to identify potential interactions between the active compounds and the polymeric components.

Antimicrobial Evaluation

The antimicrobial efficacy of the formulations was evaluated using the AATCC 100 standard method. Bacterial suspensions were adjusted to a 0.5 McFarland standard for both *S. aureus* and *E. coli*. Depending on the amount of EO or menthol in the prepared hydrogels (0.25%), adding 1, 0.5, and 0.25 grams of each Chi/HPMC-EO, Chi/HPMC-Menthol, ChiNP/HPMC-EO, and ChiNP/HPMC-Menthol to 2 mL suspension of each bacteria in a 5 cm plate, their final concentrations reached 1250, 625, and 310 µg/ml. Also, the same number of samples without EO/menthol (i.e., Chi/HPMC and ChiNP/HPMC) was added to the plates to investigate the effects of other substances in the hydrogels. After 24 hours of incubation at 37 °C, 10 µl of the suspension from each plate was cultured on an agar plate. Finally, the bacterial growth rate was calculated by comparing the colony-forming units (CFU/mL) in the control group (untreated) with those in the treated samples. All experiments were conducted in triplicate, and results are expressed as the mean ± standard deviation (SD).

In silico Study

This research employed menthol as the ligand for molecular docking studies to evaluate its potential antibacterial interactions. We obtained menthol's three-dimensional structure from the PubChem compound database (https://pubchem.ncbi.nlm.nih.gov/) and used the Avogadro program (Version 1.2, https://avogadro.cc/) to minimize energy.

We selected protein targets from two types of bacteria, *S. aureus* and *E. coli*, as they are crucial for virulence, resistance, and survival. The chosen targets comprised ClfA, FemA, FmtA, SasG, DDL, and Sortase A from *S. aureus*, as well as DHPS, DNA gyrase, and Topoisomerase IV from *E. coli*. Crystal structures of available proteins were obtained from the Protein Data Bank (PDB, https://www.rcsb.org/). Binding site prediction for proteins was performed using the PrankWeb server (https://prankweb.cz/) and also based on the positions of natural ligands present in the protein structure.

Molecular docking simulations were performed using the Molegro Virtual Docker (MVD) software. We used MolDock and Re-rank scores to determine binding affinities and hydrogen bond energies, thereby calculating the strength of the interactions. We used BIOVIA Discovery Studio Visualizer to visualize and understand protein-ligand interactions, which include hydrogen bonds, hydrophobic contacts, and π-π interactions.

RESULT

The GC-MS analysis of the *M. piperita* EO identified 14 distinct components (Table 1). After menthol (21.249%), the most predominant

Table 1. *M. piperita* EO components identified using GC-MS analysis

Retention Time	Compound	Area	%	Retention Index
9.546	α-pinene	47696251	1.100	932
11.377	β-pinene	63432312	1.269	979
13.859	limonene	195125004	3.903	1029
13.947	1,8-cineole	207426444	4.150	1026
15.662	*trans*-sabinene hydrate	47072634	1.010	1098
26.247	camphane	351577121	7.033	1131
20.004	menthone	1105246066	22.110	1152
20.299	Iso-menthone	293121099	5.864	1162
20.397	menthofuran	301336044	6.028	1164
21.249	menthol	1553773516	31.083	1172
23.985	carvone	60203623	1.204	1243
23.762	pulegone	104297121	2.086	1273
31.474	*trans*-caryophyllene	150233448	3.005	1419
33.99	germacrene D	92534749	1.851	1481

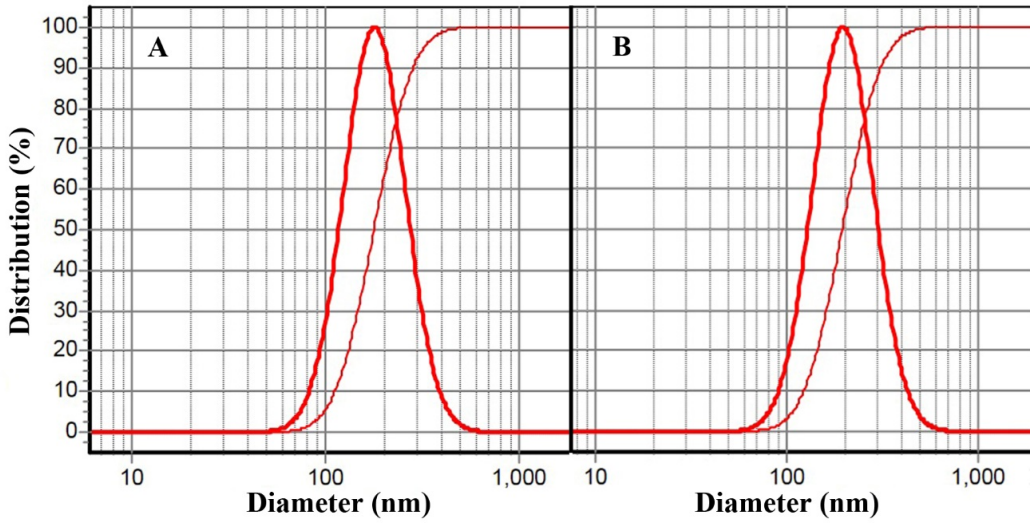

Fig. 1. DLS analysis of A: chitosan nanoparticles containing menthol, B: *M. piperita* EO EO

compounds were germacrene D, *trans*-caryophyllene, and camphane, constituting most of the EOs profile.

Chitosan Nanoparticles Containing Menthol and M. piperita EO

DLS analysis revealed that chitosan nanoparticles containing menthol had an average size of 179 ± 8 nm with a SPAN value of 0.96. In comparison, chitosan nanoparticles containing *M. piperita* EO exhibited an average size of 195 ± 6 nm with a SPAN value of 0.97 (Figure 1).

ATR-FTIR spectroscopy was used to investigate the successful incorporation of *M. piperita* EO and menthol within the prepared hydrogels. The resulting spectra are illustrated in Figure 2. ATR-FTIR analysis of *M. piperita* EO reveals key absorption bands, including a broad band at 3441 cm^{-1}, characteristic of hydrogen-bonded OH groups (alcohols and phenols like menthol), and bands at 2952, 2922, and 2868 cm^{-1} for C-H stretching vibrations. A distinct absorption at 1706 cm^{-1} and a shoulder at 1734 cm^{-1} provide evidence of the presence of carbonyl groups. Furthermore,

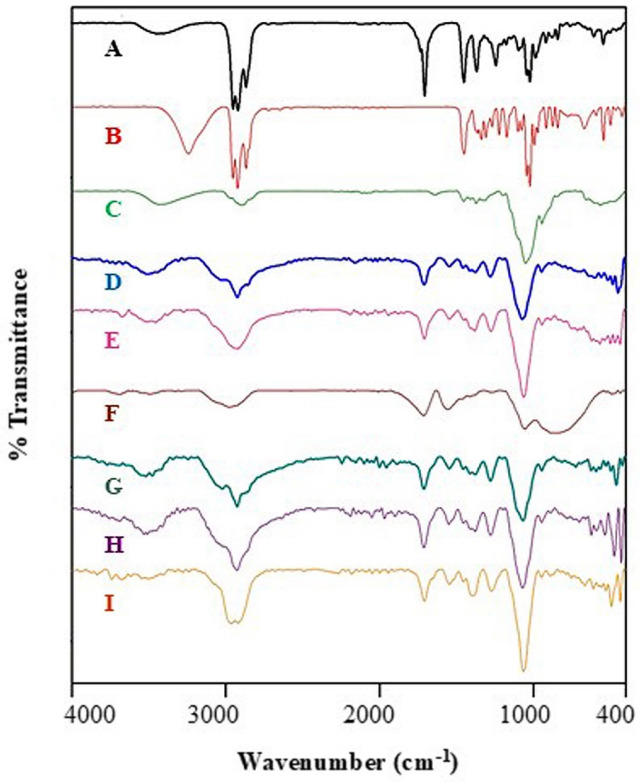

Fig. 2. ATR-FTIR spectra of A: *M. piperita* EO, B: menthol, C: HPMC, D: Chi/HPMC, E: Chi/HPMC-EO, F: Chi/HPMC-Menthol, G: ChiNP/HPMC, H: ChiNP/HPMC-EO, and I: ChiNP/HPMC-Menthol

the absorption bands at 1452 and 1369 cm^{-1} can be attributed to C-O-H, CH_3, and CH_2 bending vibrations. The bands observed at 1245, 1098, 1045, and 1024 cm^{-1} correspond to characteristic vibrations associated with C-O-C stretching and/or -CH_2- deformation modes. Additionally, the bands identified at 988, 919, 881, and 844 cm^{-1} can be attributed to out-of-plane (oop) C-H bending vibrations, typically associated with alkenes and aromatic ring structures.

The menthol spectrum exhibits the typical O-H and C-H bond absorptions at 3243, 2954, 2924, and 2869 cm^{-1}, respectively. Bending vibrations associated with C-O-H, CH_2, and CH_3 groups are identified within the 1451-1224 cm-1 range. Intense absorption bands in the 1174-995 cm^{-1} region are attributed to C-O stretching vibrations. The characteristic absorption bands of HPMC are observed at 3421 cm^{-1} (O-H stretching), 2896 cm^{-1} (C-H stretching), 1452-1312 cm^{-1} (CH_2, CH_3, and C-O-H bending), and 1051 cm^{-1} (C-O-C stretching).

The spectrum of Chi/HPMC provides significant insights into its chemical composition. A broad band at 3653- 3252 cm^{-1} indicates O-H stretching from HPMC, chitosan, and tween 20, as well as the NH_2 stretching from chitosan. Peaks at 3023, 2925, and 2856 cm^{-1} correspond to the C-H stretching vibration. A medium band at 1711 cm^{-1} is characteristic of the carbonyl groups. Other peaks at 1546, 1459, 1378, 1281, and 1073 cm^{-1} correspond to the NH, CH_2, CH_3, and C-O-H bending and C-O-C stretching vibrations, respectively.

The spectrum of Chi/HPMC-EO shows absorption bands at 3456, 2922, 1709, 1546, 1453, 1381, 1278, 1064, and 946 cm^{-1}, corresponding to O-H/NH_2, C-H, and C=O stretching, NH, CH_2, and CH_3 bending, and C-O stretching vibrations, respectively. Pique intensity, position, and shape changes indicate interactions between the hydrogel matrix and *M. piperita* EO. A red shift in the O-H stretching peak suggests hydrogen bond formation, and increased intensities of the C-H and C-O bands confirm the EO's incorporation into the hydrogel.

The Chi/HPMC-Menthol spectrum exhibits characteristic bands of both hydrogel and menthol, confirming successful menthol encapsulation. The characteristic peaks at 3487, 2979, 1715, 1556,

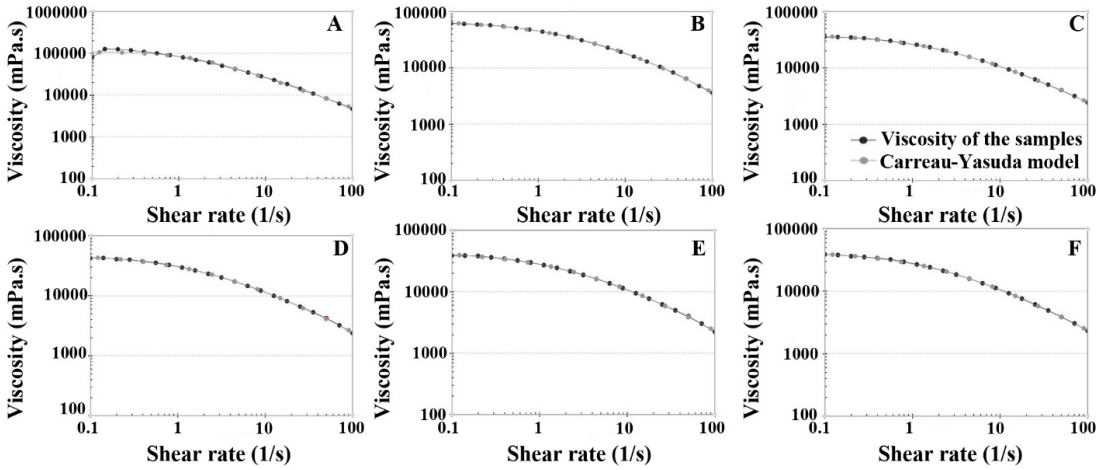

Fig. 3. Viscosity curve of A: Chi/HPMC, B: Chi/HPMC-EO, C: Chi/HPMC-Menthol, D: ChiNP/HPMC, E: ChiNP/HPMC-EO, and F: ChiNP/HPMC-Menthol

1469, 1054, and 863 cm^{-1} correspond to O-H/NH_2, C-H, C=O stretching, NH, C-O-H and CH_2/ CH_3 bending, C-O stretching, and oop C-H bending vibrations, respectively. A red shift in the O-H/NH_2 peak, increased absorption near 863 cm^{-1}, and a carbonyl peak at 1715 cm^{-1} indicate the interaction between the hydrogel matrix and menthol.

The spectrum of ChiNP/HPMC exhibits a broad band at 3670-3363 cm^{-1}, corresponding to O-H stretching and intramolecular hydrogen bonding. Asymmetric and symmetric stretching vibrations of C-H are observed at 3023 and 2926 cm^{-1}. The characteristic band at 1712 cm^{-1} is assigned to the carbonyl group. The band at 1548 cm^{-1} is likely associated with N-H bending of primary amine, while the bands at 1456, 1415, 1378, and 1280 cm^{-1} correspond to bending modes of CH_2, CH_3, and C-O-H, as well as P=O stretching vibrations of tripolyphosphate (TPP). A distinct strong band at 1068 cm-1 is also assigned to the stretching vibrations within various C-O bonds.

The ATR-FTIR spectra of ChiNP/HPMC and ChiNP/HPMC-EO show differences in peak position, shapes, and intensities, indicating interactions between the nanogel and *M. piperita* EO. Absorption bands at 3510, 2926, 1713, 1551, 1455, 1379, 1278, and 1072 cm^{-1} correspond to O-H/NH_2, C-H, and C=O stretching, N-H, C-O-H, CH_2, and CH_3 bending, P=O, and C-O stretching vibrations. A shift in the O-H/NH_2 peak suggests hydrogen bonding between the nanogel and the EO components. Enhanced C-H and C-O intensities, along with altered peak shapes, confirm the successful loading of EO into the nanogel matrix.

ATR-FTIR analysis of ChiNP/HPMC-Menthol reveals overlapping peaks from both nanogel and menthol, indicating successful encapsulation. The broad band at 3597-3373 cm^{-1} corresponds to O-H and N-H stretching with hydrogen bonding, while peaks at 2962 and 2921 cm^{-1} represent C-H vibrations. Key bands at 1709, 1546, 1455, 1395, 1274, 1067, 948, and 894 cm^{-1} are assigned to C=O and C=C stretching, N-H, C-H and O-H bending, and C-O/P=O stretching, as well as oop C-H bending vibrations. Distinct spectral changes, including a shift in the O-H/NH_2 peak, altered C-H peak shape, increased C-O intensity, and the appearance of a peak at 894 cm^{-1}, confirm the encapsulation of menthol within the nanogel.

Viscosity Analysis

Figure 3 (A–F) illustrates the viscosity profiles of the different formulations versus shear rates. In each panel, the square markers represent the experimental data, while the dashed lines indicate the Carreau–Yasuda model fitting. As observed, all formulations exhibit decreasing viscosity with increasing shear rate, indicative of a shear-thinning (non-Newtonian) behavior. This behavior is described in the Carreau–Yasuda model, which explains how changes in the structure and arrangement of polymer chains occur under various shear conditions.

Antibacterial Efficacy

The antibacterial effects of Chi/HPMC, Chi/

HPMC-EO, Chi/HPMC-Menthol, ChiNP/HPMC, ChiNP/HPMC-EO, and ChiNP/HPMC-Menthol were evaluated against *E. coli* and *S. aureus* at concentrations of 310, 625, and 1250 µg/mL (Figures 4 and 5). For *E. coli*, the control group exhibited 100% bacterial viability across all concentrations, indicating no intrinsic resistance to the treatment. Similarly, Chi/HPMC and ChiNP/HPMC matrices showed minimal antibacterial effects, with viability exceeding 90%. In contrast, adding Chi/HPMC-EO and Chi/HPMC-Menthol significantly enhanced antibacterial activity, reducing *E. coli* viability to about 5% at 1250 µg/mL. The chitosan nanoparticle-based formulations (ChiNP/HPMC-EO and ChiNP/HPMC-Menthol) demonstrated even greater potency, with bacterial viability reduced to approximately 1%.

A comparable trend was observed against *S.*

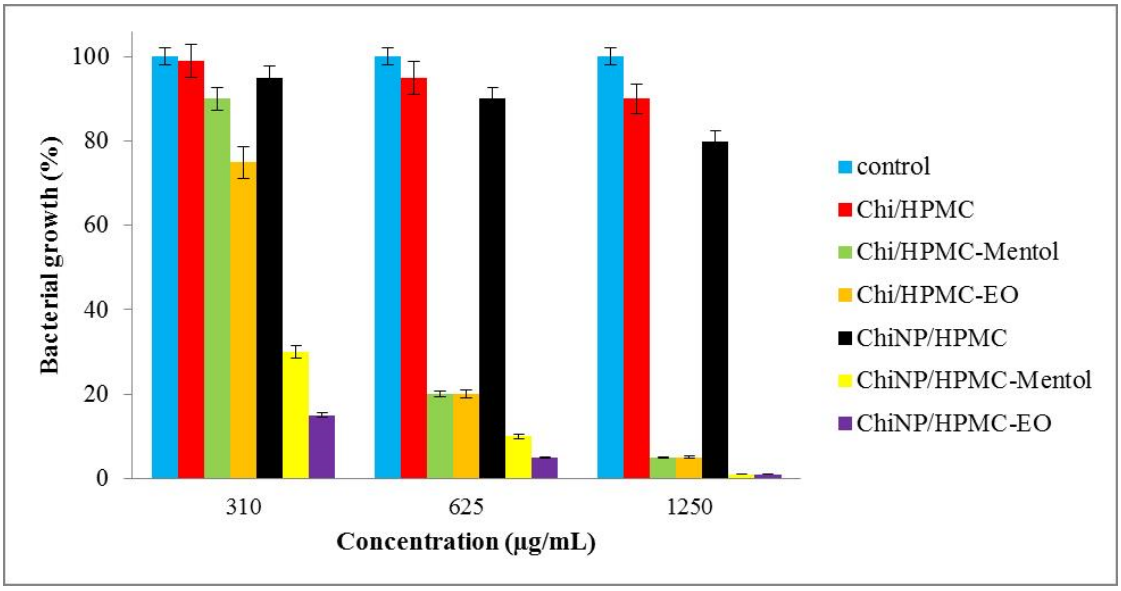

Fig. 4. Antibacterial effects of samples against *E. coli*

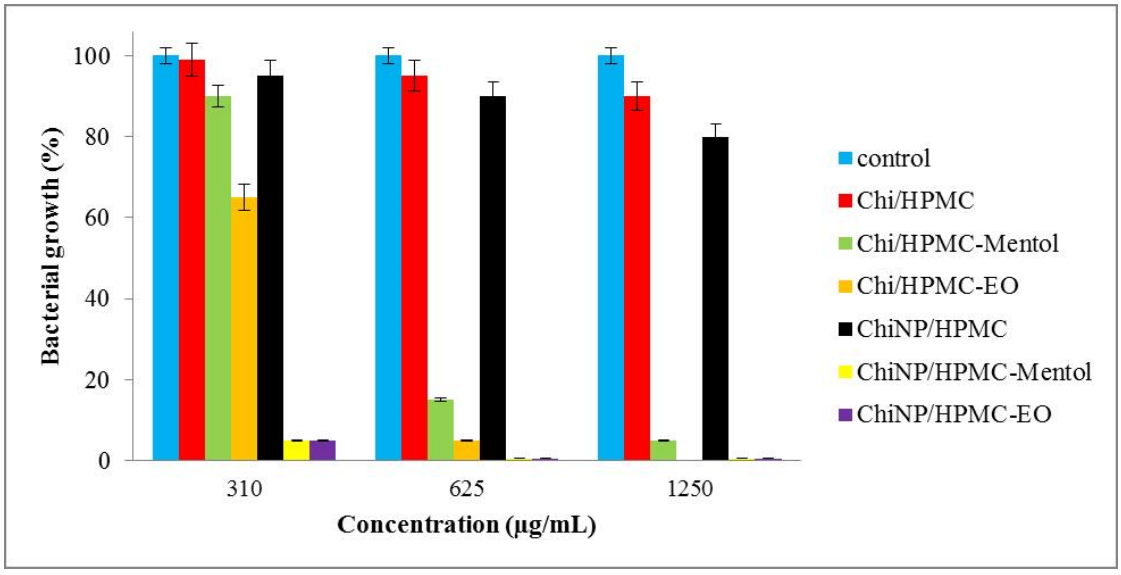

Fig. 5. Antibacterial effects of samples against *S. aureus*

aureus, though the inhibition was generally more pronounced. The control group again demonstrated 100% viability at all concentrations, whereas the Chi/HPMC and ChiNP/HPMC exhibited minimal antibacterial effects. At 1250 µg/mL, Chi/HPMC-Menthol reduced *S. aureus* viability to around 5%, whereas Chi/HPMC-EO achieved complete bacterial eradication. Notably, the nanoparticle-based formulations (ChiNP/HPMC-Menthol and ChiNP/HPMC-EO) exhibited the most vigorous activity, reducing viability to approximately 5% at the lowest tested concentration (310 µg/mL) and nearly eliminating bacterial growth (0.5% viability) at higher concentrations. These findings indicate that *S. aureus* is more susceptible than *E. coli*, aligning with earlier reports that Gram-positive bacteria—owing to their more straightforward cell wall structure—are generally more vulnerable to EOs and natural antimicrobial agents.

Molecular docking results

Molecular docking results showed that menthol formed favorable interactions with all selected target proteins from *S. aureus* and *E. coli*. As shown in Table 2, menthol showed the highest binding affinity for the FmtA protein from *S. aureus* (with a MolDock score of −78.6 kcal/mol and a Rerank score of −70.1 kcal/mol). This was followed by DNA gyrase from *E. coli* (−71.1 kcal/mol; −61.6 kcal/mol) and ClfA from *S. aureus* (−70.1 kcal/mol; −55.0 kcal/mol). Additionally, the enzymes D-alanine–D-alanine ligase and Sortase A exhibited significant binding energies, suggesting the potential for inhibiting cell wall synthesis and protein binding to the membrane. The number of hydrogen bonds varied between 1 and 5, indicating the stability and specificity of the ligand-receptor complexes.

According to the observed protein-ligand complexes in Figures 6 and 7, menthol is located in the active site of the proteins in all the studied targets and establishes stable interactions. These interactions primarily involve hydrogen bonds with polar residues, as well as hydrophobic and π–π or π–alkyl contacts with nonpolar residues within the active site. In most targets, menthol is fixed deep in the active cavity. It is surrounded by several amino acid residues, which stabilize the complex through van der Waals forces and hydrophobic interactions. Examination of 3D models by docking reveals that this type of interaction pattern is similar in most of the studied proteins and plays a crucial role in maintaining the equilibrium and stability of the ligand in the binding environment.

DISCUSSION

Antimicrobial resistance (AMR) remains one of the most pressing challenges facing global healthcare systems. In this context, medicinal plants and their bioactive compounds have attracted growing attention as potential alternative antimicrobial agents [23, 24]. Essential oils (EOs), complex mixtures of volatile secondary metabolites derived from aromatic plants, exhibit diverse bioactivities that are often attributed to their major constituents [25, 26]. A central question in this field is whether the whole EO exerts greater efficacy than its isolated active components. The literature presents varied conclusions; for instance, while *Tanacetum balsamita* EO demonstrated greater larvicidal potency than its component carvone [27]. Similarly, the isolated compound α-pinene showed more substantial anticancer effects than its source, *Rosmarinus officinalis* EO [28]. In another study, *Cymbopogon citratus* EO and its major component, citral, exhibited IC50 values of 1760 and 380 µg/

Table 2. Binding energy scores (MolDock and Re-rank) and hydrogen bonds from molecular docking of menthol with bacterial target proteins of *S. aureus* and *E. coli*

Organism	Targets	Ligands	MolDock score, kcal/mol	Rerank score, kcal/mol	HBond
E. coli	Dihydropteroate synthase	Menthol	-67.1	-58.0	-2.5
	DNA gyrase	Menthol	-71.1	-61.6	-2.0
	Topoisomerase IV	Menthol	-68.7	-60.5	-2.9
S. aureus	Clump factor A	Menthol	-70.1	-55.0	-1.7
	D-alanine-D-alanine ligase	Menthol	-69.7	-60.3	-5.0
	Sortase A	Menthol	-60.0	-52.4	-5.0
	SasG	Menthol	-65.3	-54.2	-3.1
	FmtA	Menthol	-78.6	-70.1	-1.2
	FemA	Menthol	-60.9	-50.0	-2.5

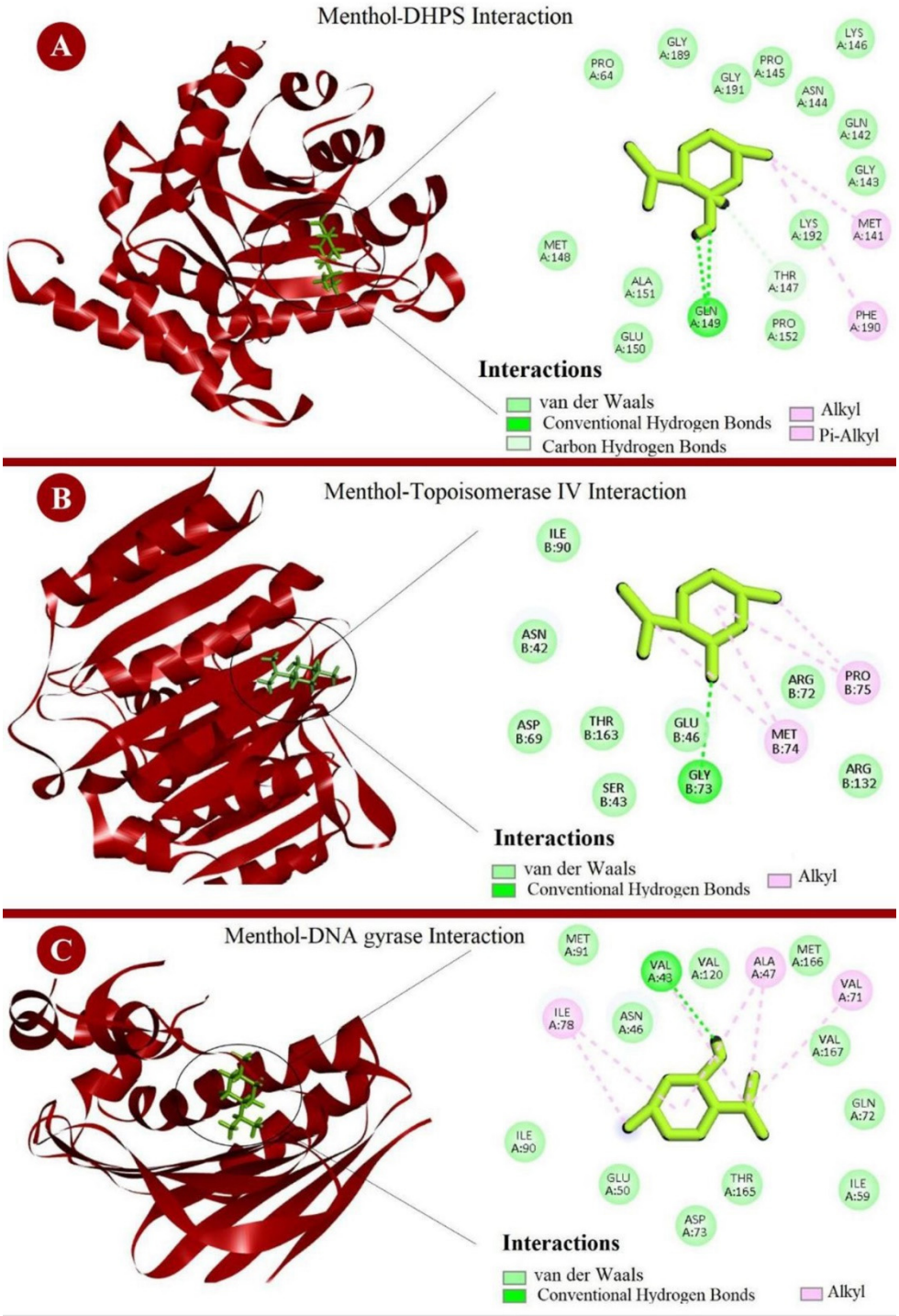

Fig. 6. Two- and three-dimensional views of the interaction of menthol in the active site of the DHPS (A), Topoisomerase IV (B), and DNA gyrase (C) proteins from *E. coli*. Hydrogen bonds and hydrophobic interactions between the ligand and amino acid residues are identified.

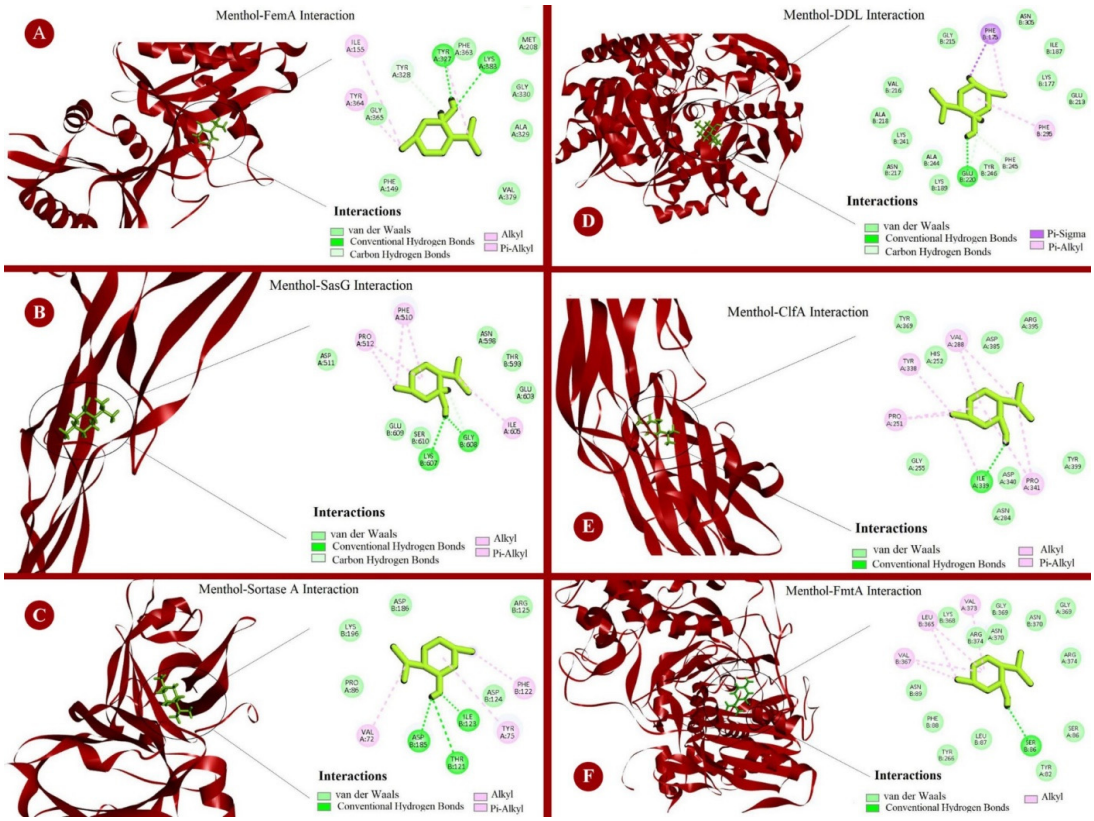

Fig. 7. Two- and three-dimensional views of the interaction of menthol in the active site of the FemA (A), SasG (B), Sortase A (C), DDL (D), CIFA (E), and FmtA (F) proteins from *S. aureus*. Hydrogen bonds and hydrophobic interactions between the ligand and amino acid residues are identified.

mL against MDA-MB-231 breast cancer cells [29]. Similarly, the antibacterial activity of *Syzygium aromaticum* EO and eugenol varies considerably depending on the specific microbial target [30, 31]. These comparative studies underscore the necessity of evaluating both whole EOs and their primary constituents.

In our study, both ChiNP/HPMC-Menthol and ChiNP/HPMC-EO exhibited potent antibacterial activity, with the latter showing marginally superior efficacy against *S. aureus*. This aligns with the existing body of evidence, suggesting that the relative effectiveness of an EO versus its principal components is highly dependent on the specific microorganism being targeted.

The antimicrobial mechanisms of EOs and plant-based compounds represent a dynamic area of research. These natural agents interact with microorganisms at the molecular level, offering novel strategies to counter antibiotic resistance [32, 33]. The activity of *M. piperita* EO and menthol involves multiple pathways that target bacterial viability. As a lipophilic monoterpene, menthol can integrate into and disrupt bacterial membrane integrity, increasing permeability and leading to the leakage of vital intracellular components, ultimately causing cell death [34, 35]. The whole EO, rich in monoterpenes, exerts a similar effect on membrane integrity. Gram-positive bacteria, such as *S. aureus*, are generally more susceptible to this action due to their simpler membrane architecture. In contrast, the complex outer membrane of Gram-negative bacteria, like *E. coli*, can confer greater resistance [36, 37]. Beyond membrane disruption, these compounds can interfere with biofilm formation [38, 39] and potentially disrupt intracellular targets, including enzymes and DNA replication processes [40, 41].

Nanoparticle-based delivery systems present a promising strategy to enhance the stability and bioavailability of volatile compounds. Our Dynamic Light Scattering (DLS) analysis confirmed the

formation of chitosan nanoparticles with a uniform and narrow size distribution, which is critical for controlled release and optimal bioavailability [42]. Encapsulating *M. piperita* EO and menthol within these nanoparticles serves to prevent volatilization, facilitate sustained release, and improve antimicrobial performance. The inherent physicochemical properties of chitosan further augment this effect by promoting interaction with bacterial membranes [43-45].

Rheological characterization revealed that our hydrogel formulations exhibit shear-thinning behavior, accurately described by the Carreau–Yasuda model [46]. This property is ideal for topical applications, as it ensures high viscosity at rest for stability while allowing easy spreadability under shear stress. The subsequent recovery of viscosity upon application prolongs the residence time of the active compounds at the site, thereby enhancing efficacy and enabling controlled release [47, 48].

A comparative evaluation with previous studies highlights the superior performance of our formulations. For example, while chitosan nanoparticles loaded with lemongrass EO required 1200 µg/mL to achieve 90% inhibition of *P. aeruginosa* and *S. aureus* [49]. *Zingiber officinale* EO-loaded chitosan nanoparticles showed only ~60% inhibition against *E. coli* and *S. aureus* [50]. Additionally, nanoemulsion-based gels containing camphor and thymol (1250 µg/mL) completely suppressed *the growth of P. aeruginosa* and *S. aureus*, while higher concentrations (1250–2500 µg/mL) were required to fully inhibit the growth of *Listeria monocytogenes* and *E. coli* [51]. Our formulations achieved total bacterial inhibition at significantly lower concentrations. This enhanced potency underscores the potential of our hydrogels as next-generation antimicrobial treatments.

To better understand the molecular basis of the observed antibacterial effects, molecular docking studies were performed for menthol against several essential protein targets of *S. aureus* and *E. coli*. The selected targets included *S. aureus* clumping factor A (ClfA), a surface-anchored adhesin that facilitates colonization and virulence [52]. D-alanine: D-alanine ligase (DDL), an enzyme crucial for bacterial cell wall synthesis [53]. Moreover, dihydropteroate synthase (DHPS), a key enzyme in folate biosynthesis, is inhibited by sulfonamide antibiotics that compete with p-aminobenzoic acid (pABA) [54].

Additional targets included FemA and FmtA—factors associated with methicillin resistance in *S. aureus* [55], as well as the biofilm-promoting surface protein SasG [56]. Moreover, sortase A is a transpeptidase responsible for anchoring surface proteins to the peptidoglycan layer [57]. Moreover, DNA gyrase and topoisomerase IV, both essential enzymes involved in bacterial DNA replication and supercoiling, were examined as critical antibacterial targets [58, 59].

Docking results revealed that menthol exhibited notable binding affinities with several of these proteins, stabilized through hydrogen bonding and hydrophobic interactions. These results suggest that menthol can effectively occupy active sites and potentially interfere with vital bacterial functions. This computational evidence corroborates previous experimental findings, which show menthol's vigorous antibacterial activity against both Gram-positive and Gram-negative bacteria [60]. Furthermore, menthol has been reported to suppress the expression of key virulence factors such as hemolysins and toxins in *S. aureus*, indicating a possible dual mechanism of antimicrobial and anti-virulence action [61].

CONCLUSION

This study successfully demonstrates the development of chitosan nanoparticle-based hydrogels loaded with *M. piperita* EO and menthol as potent antimicrobial systems. These formulations exhibited strong antibacterial activity, achieving nearly complete inhibition of *S. aureus* and *E. coli* at low concentrations. The combination of experimental and in silico findings highlights menthol's multifaceted antibacterial potential, involving both membrane disruption and enzyme inhibition mechanisms. Taken together, these results position menthol-loaded chitosan hydrogels as promising candidates for future topical antimicrobial therapies. Further investigations, particularly in vivo efficacy and toxicity studies, are necessary to validate their safety and clinical potential for managing resistant skin infections.

ETHICS APPROVAL AND CONSENT TO PARTICIPATE

This study has been ethically approved (IR.FUMS.REC.1403.037). Since this research did not involve a human study, an informed consent form was not used.

CONSENT FOR PUBLICATION

Not applicable.

ACKNOWLEDGMENTS

Not applicable.

AVAILABILITY OF DATA AND MATERIALS

All data generated or analyzed during this study are included in this published article.

COMPETING INTERESTS

Not applicable.

FUNDING

Fasa University of Medical Sciences supported this study, grant No. 403024.

REFERENCES

1. Carbonne, A., et al., National multidrug-resistant bacteria (MDRB) surveillance in France through the RAISIN network: a 9 year experience. Journal of Antimicrobial Chemotherapy, 2013. 68(4): p. 954-959. https://doi.org/10.1093/jac/dks464
2. Poolman, J.T. and A.S. Anderson, Escherichia coli and Staphylococcus aureus: leading bacterial pathogens of healthcare associated infections and bacteremia in older-age populations. Expert Review of Vaccines, 2018. 17(7): p. 607-618. https://doi.org/10.1080/14760584.2018.1488590
3. Alav, I., J.M. Sutton, and K.M. Rahman, Role of bacterial efflux pumps in biofilm formation. Journal of Antimicrobial Chemotherapy, 2018. 73(8): p. 2003-2020. https://doi.org/10.1093/jac/dky042
4. Zimmermann, S., et al., Clinically approved drugs inhibit the Staphylococcus aureus multidrug NorA efflux pump and reduce biofilm formation. Frontiers in microbiology, 2019. 10: p. 2762. https://doi.org/10.3389/fmicb.2019.02762
5. Benzaid, C., et al., The effects of Mentha× piperita essential oil on C. albicans growth, transition, biofilm formation, and the expression of secreted aspartyl proteinases genes. Antibiotics, 2019. 8(1): p. 10. https://doi.org/10.3390/antibiotics8010010
6. Djenane, D., et al., Antioxidant and antibacterial effects of Lavandula and Mentha essential oils in minced beef inoculated with E. coli O157: H7 and S. aureus during storage at abuse refrigeration temperature. Meat science, 2012. 92(4): p. 667-674. https://doi.org/10.1016/j.meatsci.2012.06.019
7. Tavazo, Z.E., et al., In vitro Antimicrobial Effect of Punica granatum Extract versus Chlorhexidine on Streptococcus sobrinus, Streptococcus sanguinis, and Candida albicans. 2023. https://doi.org/10.52547/jrdms.8.1.18
8. Kazemi, A., et al., Peppermint and menthol: a review on their biochemistry, pharmacological activities, clinical applications, and safety considerations. Crit Rev Food Sci Nutr, 2025. 65(8): p. 1553-1578. https://doi.org/10.1080/10408398.2023.2296991
9. Flood, T.R., Menthol Use for Performance in Hot Environments. Curr Sports Med Rep, 2018. 17(4): p. 135-139. https://doi.org/10.1249/JSR.0000000000000474
10. Stevens, C.J., M.L.R. Ross, and R.M. Vogel, Development of a "Cooling" Menthol Energy Gel for Endurance Athletes: Effect of Menthol Concentration on Acceptability and Preferences. Int J Sport Nutr Exerc Metab, 2021. 31(1): p. 40-45. https://doi.org/10.1123/ijsnem.2020-0190
11. Morris, G.M. and M. Lim-Wilby, Molecular docking. Methods Mol Biol, 2008. 443: p. 365-82. https://doi.org/10.1007/978-1-59745-177-2_19
12. Meng, X.Y., et al., Molecular docking: a powerful approach for structure-based drug discovery. Curr Comput Aided Drug Des, 2011. 7(2): p. 146-57. https://doi.org/10.2174/157340911795677602
13. Zhang, Y.S. and A. Khademhosseini, Advances in engineering hydrogels. Science, 2017. 356(6337): p. eaaf3627. https://doi.org/10.1126/science.aaf3627
14. Hoffman, A.S., Hydrogels for biomedical applications. Advanced Drug Delivery Reviews, 2012. 64: p. 18-23. https://doi.org/10.1016/j.addr.2012.09.010
15. He, C., S.W. Kim, and D.S. Lee, In situ gelling stimuli-sensitive block copolymer hydrogels for drug delivery. Journal of Controlled Release, 2008. 127(3): p. 189-207. https://doi.org/10.1016/j.jconrel.2008.01.005
16. Dai, H., et al., A Temperature-Responsive Copolymer Hydrogel in Controlled Drug Delivery. Macromolecules, 2006. 39(19): p. 6584-6589. https://doi.org/10.1021/ma060486p
17. Aranaz, I., et al., Chitosan: An Overview of Its Properties and Applications. Polymers, 2021. 13(19): p. 3256. https://doi.org/10.3390/polym13193256
18. Ghadermazi, R., et al., Effect of various additives on the properties of the films and coatings derived from hydroxypropyl methylcellulose-A review. Food Science & Nutrition, 2019. 7(11): p. 3363-3377. https://doi.org/10.1002/fsn3.1206
19. Siepmann, J. and N.A. Peppas, Modeling of drug release from delivery systems based on hydroxypropyl methylcellulose (HPMC). Advanced Drug Delivery Reviews, 2012. 64: p. 163-174. https://doi.org/10.1016/j.addr.2012.09.028
20. Thoniyot, P., et al., Nanoparticle-Hydrogel Composites: Concept, Design, and Applications of These Promising, Multi-Functional Materials. Advanced Science, 2015. 2(1-2): p. 1400010. https://doi.org/10.1002/advs.201400010
21. Valizadeh, A., et al., Antibacterial effects of impregnated scaffolds with solid lipid nanoparticles gels containing three essential oils against standard and clinical strains of Pseudomonas aeruginosa and Staphylococcus aureus. Nanomedicine Research Journal 2021. 6(3): p. 218-227.
22. Osanloo, M., et al., Novel Nanocarrier for Melanoma Treatment: Chitosan-Gum Arabic Nanoparticles Containing Menthol. BioNanoScience, 2024. https://doi.org/10.1007/s12668-024-01578-8
23. Ciofu, O. and T. Tolker-Nielsen, Tolerance and resistance of Pseudomonas aeruginosa biofilms to antimicrobial agents-how P. aeruginosa can escape antibiotics. Frontiers in microbiology, 2019. 10: p. 913. https://doi.org/10.3389/fmicb.2019.00913
24. Hoceini, A., et al., Evaluation of Biofilm Forming Potential and Antimicrobial Resistance Profile of S. aureus and P. aeruginosa Isolated from Peripheral Venous Catheters and Urinary Catheters In Algeria, in vitro Study. Advanced Research in Life Sciences, 2023. 7(1): p. 83-92. https://doi.org/10.2478/arls-2023-0010
25. Romero, C.D., et al., Antibacterial properties of

common herbal remedies of the southwest. Journal of Ethnopharmacology, 2005. 99(2): p. 253-257. https://doi.org/10.1016/j.jep.2005.02.028
26. Pavithra, P., et al., Antibacterial activity of plants used in Indian herbal medicine. International Journal of Green Pharmacy, 2010. 4(1): p. 22-28. https://doi.org/10.4103/0973-8258.62161
27. Sanei-Dehkordi, A., et al., Promising Larvicidal Effects of Nanoliposomes Containing Carvone and Mentha spicata and Tanacetum balsamita Essential Oils Against Anopheles stephensi. Acta parasitologica, 2024. 69(1): p. 216-226. https://doi.org/10.1007/s11686-023-00735-5
28. Rahmani, H., et al., Chitosan nanoparticles containing α-pinene and Rosmarinus officinalis L. essential oil: effects on human melanoma cells' viability and expression of apoptosis-involved genes. Polymer Bulletin, 2024. 81(3): p. 2505-2523. https://doi.org/10.1007/s00289-023-04839-w
29. Karami, F., et al., Comparison of the efficacy of alginate nanoparticles containing Cymbopogon citratus essential oil and citral on melanoma and breast cancer cell lines under normoxic and hypoxic conditions. BMC Complementary Medicine and Therapies, 2024. 24(1): p. 372. https://doi.org/10.1186/s12906-024-04673-1
30. Valizadeh, A., et al., Anticarcinogenic Effect of Chitosan Nanoparticles Containing Syzygium aromaticum Essential Oil or Eugenol Toward Breast and Skin Cancer Cell Lines. BioNanoScience, 2021. 11(3): p. 678-686. https://doi.org/10.1007/s12668-021-00880-z
31. Moemenbellah-Fard, M., et al., Antibacterial and leishmanicidal activities of Syzygium aromaticum essential oil versus its major ingredient, eugenol. Flavour and Fragrance Journal, 2020. 35(5): p. 534-540. https://doi.org/10.1002/ffj.3595
32. Zhou, Y., et al., A review of the antibacterial activity and mechanisms of plant polysaccharides. Trends in Food Science & Technology, 2022. 123: p. 264-280. https://doi.org/10.1016/j.tifs.2022.03.020
33. Álvarez-Martínez, F.J., et al., Antibacterial plant caompounds, extracts and essential oils: An updated review on their effects and putative mechanisms of action. Phytomedicine, 2021. 90: p. 153626. https://doi.org/10.1016/j.phymed.2021.153626
34. Kamatou, G.P.P., et al., Menthol: A simple monoterpene with remarkable biological properties. Phytochemistry, 2013. 96: p. 15-25. https://doi.org/10.1016/j.phytochem.2013.08.005
35. Hudz, N., et al., Mentha piperita: Essential Oil and Extracts, Their Biological Activities, and Perspectives on the Development of New Medicinal and Cosmetic Products. Molecules, 2023. 28(21): p. 7444. https://doi.org/10.3390/molecules28217444
36. Singh, R., M.A.M. Shushni, and A. Belkheir, Antibacterial and antioxidant activities of Mentha piperita L. Arabian Journal of Chemistry, 2015. 8(3): p. 322-328. https://doi.org/10.1016/j.arabjc.2011.01.019
37. McKay, D.L. and J.B. Blumberg, A review of the bioactivity and potential health benefits of peppermint tea (Mentha piperita L.). Phytotherapy Research, 2006. 20(8): p. 619-33. https://doi.org/10.1002/ptr.1936
38. Trombetta, D., et al., Mechanisms of Antibacterial Action of Three Monoterpenes. Antimicrobial Agents and Chemotherapy, 2005. 49(6): p. 2474-2478. https://doi.org/10.1128/AAC.49.6.2474-2478.2005
39. Pergolizzi Jr, J.V., et al., The role and mechanism of action of menthol in topical analgesic products. Journal of Clinical Pharmacy and Therapeutics, 2018. 43(3): p. 313-319. https://doi.org/10.1111/jcpt.12679
40. Stewart, M.P., R. Langer, and K.F. Jensen, Intracellular Delivery by Membrane Disruption: Mechanisms, Strategies, and Concepts. Chemical reviews, 2018. 118(16): p. 7409-7531. https://doi.org/10.1021/acs.chemrev.7b00678
41. Patel, T., Y. Ishiuji, and G. Yosipovitch, Menthol: A refreshing look at this ancient compound. Journal of the American Academy of Dermatology, 2007. 57(5): p. 873-878. https://doi.org/10.1016/j.jaad.2007.04.008
42. Ashrafi, B., et al., Mentha piperita essential oils loaded in a chitosan nanogel with inhibitory effect on biofilm formation against S. mutans on the dental surface. Carbohydrate polymers, 2019. 212: p. 142-149. https://doi.org/10.1016/j.carbpol.2019.02.018
43. Esmaeili, A. and A. Asgari, In vitro release and biological activities of Carum copticum essential oil (CEO) loaded chitosan nanoparticles. International Journal of Biological Macromolecules, 2015. 81: p. 283-290. https://doi.org/10.1016/j.ijbiomac.2015.08.010
44. Khoshnevisan, K., et al., Chitosan nanoparticles containing cinnamomum verum J. Presl essential oil and cinnamaldehyde: preparation, characterization and anticancer effects against melanoma and breast cancer cells. Traditional and Integrative Medicine, 2022. 7(1): p. 1-12. https://doi.org/10.18502/tim.v7i1.9058
45. Nguyen, G. and X. Le. Palmarosa essential oil encapsulated in chitosan nanoparticles by ionotropic gelation: Formulation and characterization. in IOP Conference Series: Earth and Environmental Science. 2021. IOP Publishing. https://doi.org/10.1088/1755-1315/947/1/012002
46. Zare, Y., S.P. Park, and K.Y. Rhee, Analysis of complex viscosity and shear thinning behavior in poly (lactic acid)/poly (ethylene oxide)/carbon nanotubes biosensor based on Carreau-Yasuda model. Results in Physics, 2019. 13: p. 102245. https://doi.org/10.1016/j.rinp.2019.102245
47. Damiri, F., et al., Synthesis and characterization of Lyophilized chitosan-based hydrogels cross-linked with benzaldehyde for controlled drug release. Journal of Chemistry, 2020. 2020(1): p. 8747639. https://doi.org/10.1155/2020/8747639
48. Müller, S.J., et al., Flow and hydrodynamic shear stress inside a printing needle during biofabrication. PLoS One, 2020. 15(7): p. e0236371. https://doi.org/10.1371/journal.pone.0236371
49. Noorbakhsh, F., et al., Preparation, Characterization, and Antibacterial Evaluation of Nanoemulsions and Chitosan Nanoparticles Containing Lemongrass Essential Oil and Citral against Staphylococcus aureus and Pseudomonas aeruginosa. BioNanoScience, 2025. 15(1): p. 210. https://doi.org/10.1007/s12668-025-01841-6
50. Zarenezhad, E., et al., Development of Alginate and Chitosan Nanoparticles as Carriers of Zingiber officinale Essential Oil for Enhancement of Its Anticancer, Antibacterial, and Antifungal Activities. BioNanoScience, 2024. https://doi.org/10.1007/s12668-024-01478-x
51. Abdollahi, A., et al., Nanoformulated herbal compounds: enhanced antibacterial efficacy of camphor and thymol-loaded nanogels. BMC Complementary Medicine and Therapies, 2024. 24(1): p. 138. https://doi.org/10.1186/s12906-024-04435-z
52. Herman-Bausier, P., et al., Staphylococcus aureus

clumping factor A is a force-sensitive molecular switch that activates bacterial adhesion. Proc Natl Acad Sci U S A, 2018. 115(21): p. 5564-5569. https://doi.org/10.1073/pnas.1718104115
53. Liu, S., et al., Allosteric inhibition of Staphylococcus aureus D-alanine:D-alanine ligase revealed by crystallographic studies. Proc Natl Acad Sci U S A, 2006. 103(41): p. 15178-83. https://doi.org/10.1073/pnas.0604905103
54. Dennis, M.L., et al., 8-Mercaptoguanine Derivatives as Inhibitors of Dihydropteroate Synthase. Chemistry, 2018. 24(8): p. 1922-1930. https://doi.org/10.1002/chem.201704730
55. Rahman, M.M., et al., The Staphylococcus aureus Methicillin Resistance Factor FmtA Is a d-Amino Esterase That Acts on Teichoic Acids. mBio, 2016. 7(1): p. e02070-15. https://doi.org/10.1128/mBio.02070-15
56. Geoghegan, J.A., et al., Role of surface protein SasG in biofilm formation by Staphylococcus aureus. J Bacteriol, 2010. 192(21): p. 5663-73. https://doi.org/10.1128/JB.00628-10
57. Mazmanian, S.K., et al., Staphylococcus aureus sortase mutants defective in the display of surface proteins and in the pathogenesis of animal infections. Proc Natl Acad Sci U S A, 2000. 97(10): p. 5510-5. https://doi.org/10.1073/pnas.080520697
58. Jakhar, R., et al., Discovery of Novel Inhibitors of Bacterial DNA Gyrase Using a QSAR-Based Approach. ACS Omega, 2022. 7(36): p. 32665-32678. https://doi.org/10.1021/acsomega.2c04310
59. Li, Y., et al., Characterization of the interaction between Escherichia coli topoisomerase IV E subunit and an ATP competitive inhibitor. Biochem Biophys Res Commun, 2015. 467(4): p. 961-6. https://doi.org/10.1016/j.bbrc.2015.10.036
60. Al-Bayati, F.A., Isolation and identification of antimicrobial compound from Mentha longifolia L. leaves grown wild in Iraq. Ann Clin Microbiol Antimicrob, 2009. 8: p. 20. https://doi.org/10.1186/1476-0711-8-20
61. Qiu, J., et al., Menthol diminishes Staphylococcus aureus virulence-associated extracellular proteins expression. Appl Microbiol Biotechnol, 2011. 90(2): p. 705-12. https://doi.org/10.1007/s00253-011-3122-9